



# *Toxoplasma gondii* Toxolysin 4 Contributes to Efficient Parasite Egress from Host Cells

My-Hang Huynh,<sup>a</sup>  Marijo S. Roiko,<sup>a\*</sup> Angelica O. Gomes,<sup>a\*</sup> Ellyn N. Schinke,<sup>a</sup> Aric J. Schultz,<sup>a\*</sup> Swati Agrawal,<sup>a\*</sup> Christine A. Oellig,<sup>c</sup> Travis R. Sexton,<sup>d</sup> Jessica M. Beauchamp,<sup>a\*</sup> Julie Laliberté,<sup>a</sup> Komagal Kannan Sivaraman,<sup>c</sup> Louis B. Hersh,<sup>b</sup> Sheena McGowan,<sup>c</sup>  Vern B. Carruthers<sup>a</sup>

<sup>a</sup>Department of Microbiology and Immunology, University of Michigan Medical School, Ann Arbor, Michigan, USA

<sup>b</sup>Department of Molecular and Cellular Biochemistry and Center for Structural Biology, University of Kentucky, Lexington, Kentucky, USA

<sup>c</sup>Infection and Immunity Program, Biomedicine Discovery Institute, Department of Microbiology, Monash University, Clayton, Victoria, Australia

<sup>d</sup>Department of Cardiology, University of Kentucky, Lexington, Kentucky, USA

**ABSTRACT** Egress from host cells is an essential step in the lytic cycle of *T. gondii* and other apicomplexan parasites; however, only a few parasite secretory proteins are known to affect this process. The putative metalloproteinase toxolysin 4 (TLN4) was previously shown to be an extensively processed microneme protein, but further characterization was impeded by the inability to genetically ablate *TLN4*. Here, we show that TLN4 has the structural properties of an M16 family metalloproteinase, that it possesses proteolytic activity on a model substrate, and that genetic disruption of *TLN4* reduces the efficiency of egress from host cells. Complementation of the knockout strain with the *TLN4* coding sequence significantly restored egress competency, affirming that the phenotype of the  $\Delta tln4$  parasite was due to the absence of TLN4. This work identifies TLN4 as the first metalloproteinase and the second microneme protein to function in *T. gondii* egress. The study also lays a foundation for future mechanistic studies defining the precise role of TLN4 in parasite exit from host cells.

**IMPORTANCE** After replicating within infected host cells, the single-celled parasite *Toxoplasma gondii* must rupture out of such cells in a process termed egress. Although it is known that *T. gondii* egress is an active event that involves disruption of host-derived membranes surrounding the parasite, very few proteins that are released by the parasite are known to facilitate egress. In this study, we identify a parasite secretory protease that is necessary for efficient and timely egress, laying the foundation for understanding precisely how this protease facilitates *T. gondii* exit from host cells.

**KEYWORDS** *Toxoplasma gondii*, apicomplexan parasites, egress, intracellular parasites, proteases

Egress by apicomplexan parasites, including *Toxoplasma gondii* and malaria parasites (*Plasmodium* spp.), is the critical last step in the lytic cycle. Egress liberates the parasite for infection of new cells and releases host cell cytosolic contents, which can activate an inflammatory immune response (1). Inflammation is a hallmark of toxoplasmosis, with associated ocular, neural, cardiac, or respiratory disease, which is especially severe in immunodeficient or congenitally infected individuals. Severe inflammation during toxoplasmosis is linked to the parasite genotype, with highly virulent strains being associated with worse outcome, especially for ocular and congenital infection (2).

Recent focus on egress is elucidating signaling pathways and associated secondary messengers, providing a broader understanding of the intricate interplay between the signals involved in this complex cascade of events (recently reviewed in reference 3).

**Citation** Huynh M-H, Roiko MS, Gomes AO, Schinke EN, Schultz AJ, Agrawal S, Oellig CA, Sexton TR, Beauchamp JM, Laliberté J, Sivaraman KK, Hersh LB, McGowan S, Carruthers VB. 2021. *Toxoplasma gondii* toxolysin 4 contributes to efficient parasite egress from host cells. mSphere 6:e00444-21. <https://doi.org/10.1128/mSphere.00444-21>.

**Editor** William J. Sullivan, Indiana University School of Medicine

**Copyright** © 2021 Huynh et al. This is an open-access article distributed under the terms of the [Creative Commons Attribution 4.0 International license](https://creativecommons.org/licenses/by/4.0/).

Address correspondence to Vern B. Carruthers, [vcarruth@umich.edu](mailto:vcarruth@umich.edu).

\* Present address: Marijo S. Roiko, Department of Pathology and Laboratory Services, Altru Health System, Grand Forks, North Dakota, USA; Angelica O. Gomes, Departamento de Biologia Estrutural, Universidade Federal do Triângulo Mineiro, Uberaba, Brazil; Aric J. Schultz, Lumicks Inc., Waltham, Massachusetts, USA; Swati Agrawal, Department of Biology, University of Mary Washington, Fredericksburg, Virginia, USA; Jessica M. Beauchamp, Department of Microbiology and Immunology, University of North Carolina, Chapel Hill, Chapel Hill, North Carolina, USA.

 New work from the Carruthers lab @VernCarruthers shows that the single-celled parasite *Toxoplasma gondii* uses a protease to help it exit from host cells.

**Received** 12 May 2021

**Accepted** 9 June 2021

**Published** 30 June 2021

Such studies have solidified roles for cyclic GMP (cGMP) and calcium to stimulate protein kinase G (PKG) (4, 5) and calcium-dependent protein kinases (CDPKs) (4, 6–8), among other targets. Calcium signaling results in the activation of parasite motility and the discharge of apical secretory granules, termed micronemes (9–12). While the importance of microneme proteins, such as transmembrane adhesins that connect with the actin-myosin motor system to drive gliding motility and active cell invasion, have been established, microneme proteins also contribute to active egress via their role in the formation of pores such as those created by Perforin-like protein 1 (PLP1) (13–15). Gene knockout (KO) studies suggest that PLP1 pore formation disrupts the parasitophorous vacuole membrane (PVM), which encases parasites during intracellular replication. *PLP1*-deficient parasites are delayed or fail in egress and show a marked loss of virulence in infected mice, implying a link between efficient egress and virulence. Although several proteins released from parasite-dense granules (calcium-independent secretory organelles released during parasite replication) have also been implicated in egress (16–20), PLP1 is the only microneme protein known to directly function in egress to date.

Previous work identified a putative metalloprotease, toxolysin 4 (TLN4; TGME49\_206510), in a proteomic screen of *Toxoplasma* secretory products released by extracellular tachyzoites (21). A subsequent study showed that TLN4 is a microneme protein that undergoes extensive proteolytic processing and potentially contributes to parasite fitness, based on loss of *TLN4*-deficient parasites from a mixed population of parasites transfected with a knockout plasmid (22). However, a recent genome-wide CRISPR/Cas9 knockout screen indicated that TLN4 does not contribute substantially to parasite fitness based on its phenotype score of 0.51 (on a scale of –7 to 3, with lower values indicating lower fitness) (23). TLN4 is a member of the M16 metalloproteinase subfamily of so-called cryptases, which are represented throughout the tree of life and include four TLN genes in the *Toxoplasma* genome. M16 metalloproteinases are exemplified by the human insulin-degrading enzyme (IDE) and feature a catalytic chamber (or crypt) that accommodates small polypeptides for degradation. Whereas characterization of TLN2 (TGME49\_227948) and TLN3 (TGME49\_257010) has not been reported, TLN1 (TGME49\_269885) resides in the parasite secretory rhoptries, where it plays an unknown role apart from contributing modestly to growth *in vitro* (24).

Here, we show that TLN4 has the structural features of an active metalloproteinase and that it possesses proteolytic activity against a model polypeptide substrate. We also report that *TLN4*-deficient parasites show normal gliding motility, cell invasion, and replication but have a delayed induced-egress phenotype. Our findings suggest that TLN4 contributes to *Toxoplasma* egress, identifying it as only the second microneme protein implicated in this event.

## RESULTS

**TLN4 has the structural features of an active metalloproteinase.** TLN4 is a large (2,435-amino-acid [aa]) protein that contains multiple domains, including one active (A) and three inactive (IA) M16 proteinase domains, along with a long C-terminal extension that includes a repeat domain consisting of eight tandem repeats of a 28-aa sequence (Fig. 1A). Structural modeling of the M16 proteinase domains (residues 202 to 1367) using the human insulin-degrading enzyme as a template suggests that each domain forms a similar  $\alpha\beta$  roll fold, with the domains arranged around a central chamber (Fig. 1B), as expected for an M16 family metalloproteinase (25). When viewed from a perspective of inside the chamber or crypt, a putative active site is visible (Fig. 1C) with the characteristic HXXEHX<sub>n</sub>EX<sub>6</sub>E binding motif for catalytic Zn<sup>2+</sup> arranged on two  $\alpha$ -helices (Fig. 1D) that are separated by 60 amino acids in TLN4 (Fig. 1E). These features are consistent with TLN4 being an active metalloproteinase of the M16 family.

**Recombinant TLN4 is capable of processing  $\beta$ -insulin.** M16 family proteinases typically act upon peptides and polypeptides that are sufficiently small to fit in the crypt. To determine if TLN4 possesses proteolytic activity, we expressed and purified a recombinant form of TLN4 lacking the C-terminal extension. TLN4<sub>209–1295</sub> was expressed

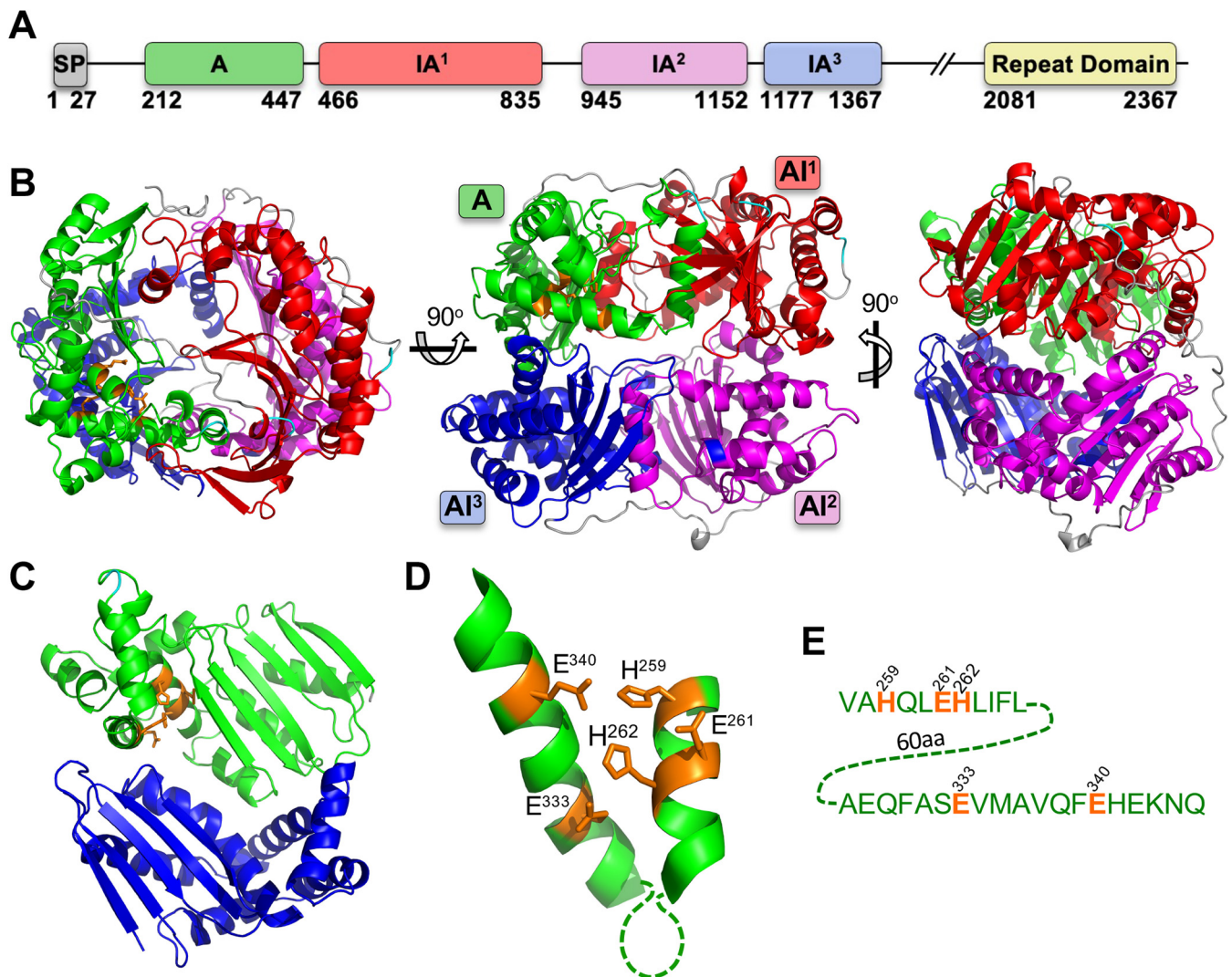


**FIG 1** Structural features of TLN4. (A) Domain structure of TLN4 illustrating its possession of a signal peptide (SP) and, based on the IDE structure, a single active domain (domain A), 3 inactive domains (IA<sup>1-3</sup>), and a C-terminal repeat domain. Note that a largely featureless region between IA<sup>3</sup> and the repeat domain is not shown and is instead denoted by //. Numbering indicates amino acid positions and is based on the sequenced cDNA of TLN4 (22). (B) Structural model of TLN4 showing the arrangement of domains into a shell surrounding a central catalytic chamber. Three different views are provided. (C) The A and IA<sup>3</sup> domains viewed from the center of the chamber with residues that coordinate zinc binding shown in orange. (D) Zoom-in of the adjacent alpha helices of the A domain showing the residues (orange) that are predicted to coordinate binding to zinc. (E) Sequence of the alpha helices shown in panel D, including residues (orange) that likely mediate binding to zinc as a cofactor for proteolytic activity.

using a bacterial expression system and was purified and refolded. The purified protein migrated on SDS-PAGE as a prominent 130-kDa band and behaved as a monodispersed protein when analyzed by size exclusion chromatography (Fig. 2A). Upon incubating recombinant TLN4 with  $\beta$ -insulin as a model substrate, we observed the generation of several cleavage products (Fig. 2B), which were confirmed by mass spectrometry to originate from  $\beta$ -insulin (Fig. 2C). Mapping of the cleavage sites on the sequence of  $\beta$ -insulin revealed a preference for TLN4 cleavage in the central region of the polypeptide but no obvious preference for recognition of specific amino acids. Collectively, our findings suggest that TLN4 is an active protease that is capable of processing a model substrate.

**TLN4 is amenable to genetic disruption.** In a previous study of TLN4, it was proposed that TLN4 contributes to parasite fitness, because TLN4-knockout parasites could be detected in a population of transfected RH parasites but were lost through further culturing (22). To enhance the recovery of knockout parasites, we utilized RH $\Delta ku80\Delta hcg$  parasites (wild type [WT] here) and transfected them with a

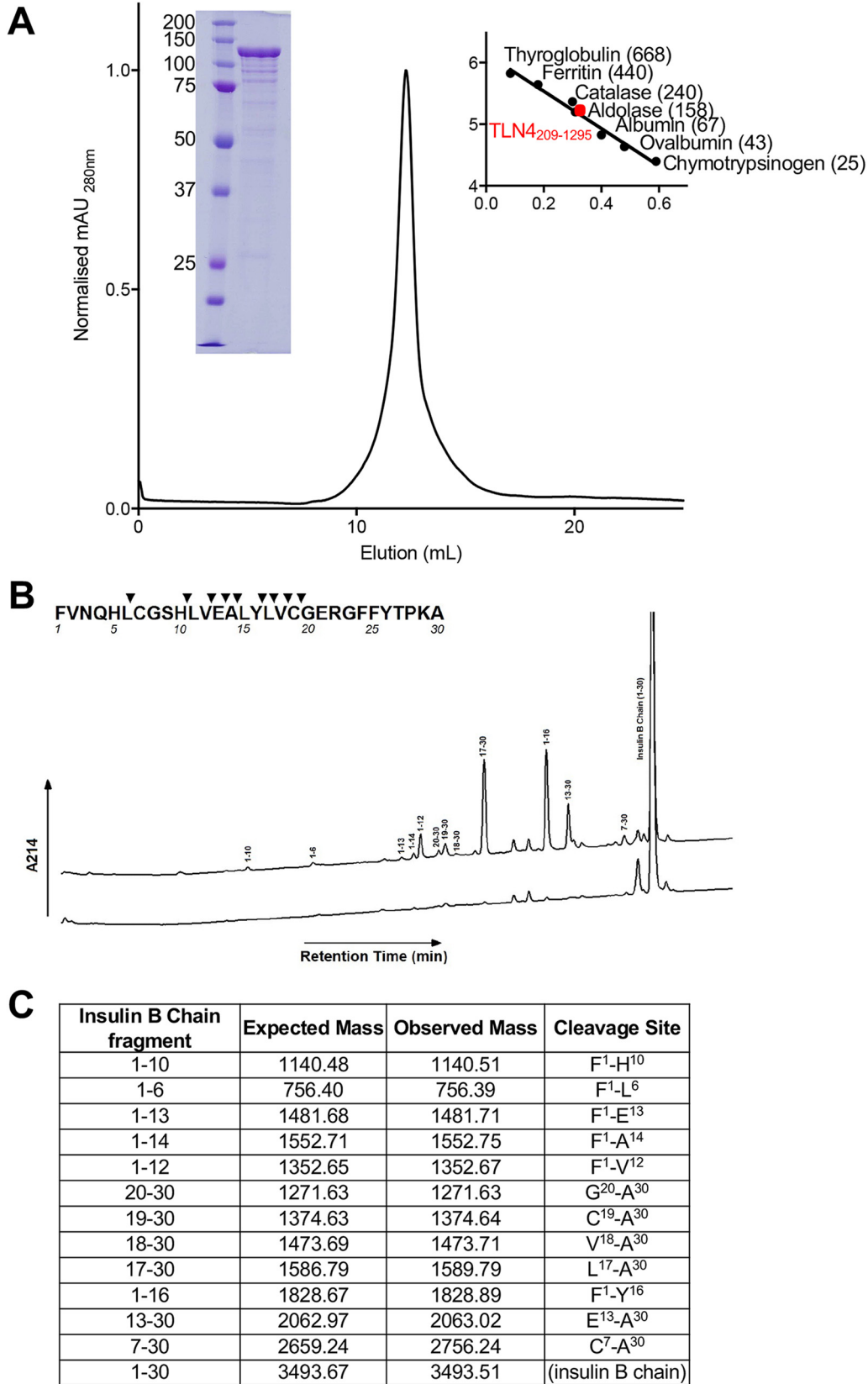


**FIG 2** Recombinant TLN4 proteolytic activity using  $\beta$ -insulin as a model substrate. (A) Chromatogram showing the elution of recombinant TLN4 as a monodispersed peak from size exclusion chromatography. SDS-PAGE of purified TLN4 is shown inset on the left, with molecular weight markers indicated on the right of the elution peak. Values in (Continued on next page)

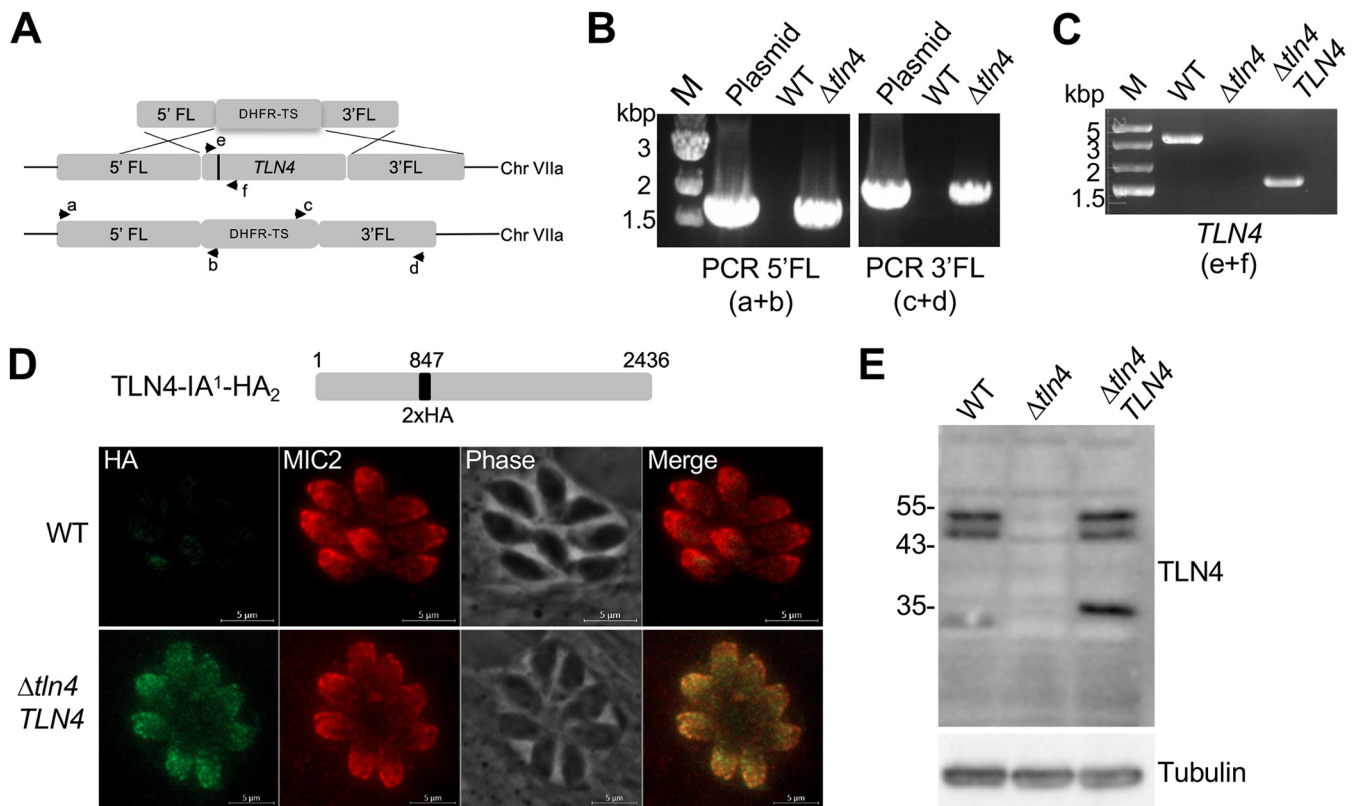


**FIG 3** Genetic disruption of *TLN4*. (A) Schematic showing the *TLN4* genomic locus and homologous recombination with a cassette containing a *TLN4* 5' flank, the HXGPRT selectable marker, and a *TLN4* 3' flank. Arrows and letters indicate the placement of primers used in panel B, and the black bar in *TLN4* indicates an intron that permits distinction of the gene from the cDNA in panel C. Other introns of *TLN4* are not shown. (B) PCR validation of selectable marker integration at the 5' (primers a and b) and 3' (primers c and d) end. M, molecular weight marker. (C) PCR validation of *TLN4* deletion ( $\Delta tln4$ ) and complementation ( $\Delta tln4TLN4$ ) with the cDNA (primers e and f). The differences in size are due to the presence of an intron in the WT genomic DNA versus the cDNA in the complement strain lacking the intron. (D) Schematic showing the complementation construct with a 2 $\times$  HA tag in the full-length *TLN4* coding sequence. The immunofluorescence panel shows the micronemal localization of the complemented strain, costained with anti-MIC2. (E) Mouse antibodies to *TLN4* detect the ~55-kDa doublet and the ~32 kDa of *TLN4* in the lysates of WT and  $\Delta tln4TLN4$  parasites. Slower mobility of the smallest band in the complement strain is due to the HA tag. Sizes (in kilodaltons) of molecular weight markers are shown to the left. Detection of *T. gondii* tubulin was included as a loading control.

hypoxanthine xanthine guanine phosphoribosyl transferase (HXGPRT) selectable cassette flanked by 5' and 3' *TLN4* homology regions (Fig. 3A). Individual knockout parasite clones were tested by PCR for integration of the selectable marker at the 5' and 3' ends (Fig. 3B) and for the absence of the *TLN4* gene ( $\Delta tln4$ ) (Fig. 3C). We then genetically complemented  $\Delta tln4$  parasites by expression of the *TNL4* cDNA containing two copies of a hemagglutinin (HA) epitope tag inserted at aa 847 after the first inactive domain (TLN4-IA<sup>1</sup>-HA<sub>2</sub>) to generate  $\Delta tln4TLN4$  parasites, which were confirmed by PCR (Fig. 3C). The difference in fragment size in the WT and  $\Delta tln4TLN4$  parasites is due to the presence of introns in the WT but not in the cDNA of the complement strain. Expression of *TLN4* in  $\Delta tln4TLN4$  parasites was confirmed by fluorescence microscopy (Fig. 3D). We further validated expression by Western blotting, which showed the expected doublet of processed *TLN4* at ~50 kDa and a smaller ~35-kDa species (Fig. 3E). This smaller species showed the expected increase in size in  $\Delta tln4TLN4$  due to the HA tag. The loss of the *TLN4* protein in  $\Delta tln4$  was also confirmed by Western blotting (Fig. 3E).

**FIG 2** Legend (Continued)

parentheses indicate molecular size in kDa. (B) HPLC profile of insulin B chain cleaved by *TLN4*. Hydrolysis products were determined by comparing a reaction allowed to incubate (top line) versus a reaction that was immediately stopped (bottom line). (Inset) Captured peaks are labeled with their residue number, and a cleavage map was developed. (C) Mass spectrometry analysis of captured hydrolysis products from insulin B chain are shown with their expected mass and observed mass along with the fragment and cleavage sites that each product represents.

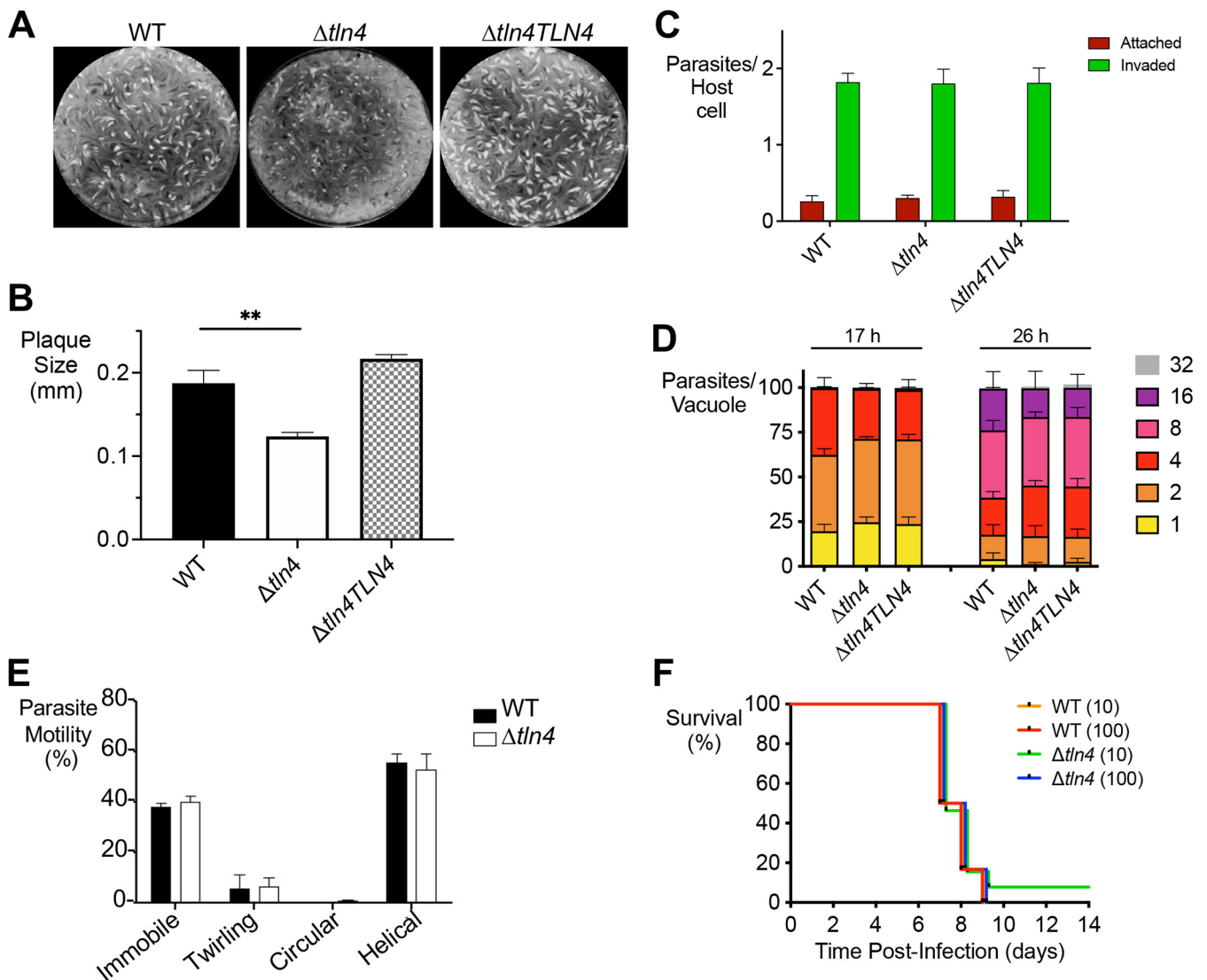


**FIG 4** Effect of TLN4-deficient parasites on the lytic cycle. (A) Plaque assays show smaller plaques in  $\Delta tln4$  parasites. One hundred parasites of each strain were inoculated into 6-well plates and allowed to grow for 7 days undisturbed. Wells were stained with crystal violet. (B) Individual plaque sizes were measured using ImageJ. Data represent three independent biological experiments with triplicate samples within each experiment. A minimum of 500 plaques were counted per strain. Error bars represent standard errors of the means (SEM), and statistics were performed using an unpaired, two-tailed, Student's *t* test. (C) Parasites lacking TLN4 show normal invasion. HFF cells in 8-well chamber slides were inoculated with parental,  $\Delta tln4$ , or  $\Delta tln4TLN4$  parasites and allowed to invade for 20 min prior to fixation. Wells were differentially stained with SAG1 antibodies to detect attached or invaded parasites per host cell nucleus. A minimum of 250 host cells were counted per strain. Data in the invasion (C) and replication (D) graphs represent means  $\pm$  SEM from three independent experiments, each with triplicate samples. At least 8 fields of view were counted per well. (D) Parasites lacking TLN4 replicate normally. Parasites were inoculated into 8-well chamber slides and allowed to replicate for 17 h or 26 h prior to fixation and enumeration of parasites per vacuole. A minimum of 250 vacuoles were counted per strain per time point. (E)  $\Delta tln4$  parasites show normal modes of gliding motility. Video microscopy to enumerate the types of gliding motility shows the percentages of immobile parasites and parasites performing twirling, circular, and helical gliding in all strains tested. Graphs indicate the means  $\pm$  SEM from three independent experiments. \*,  $P \leq 0.05$  by Student's *t* test. (F) TLN4 does not play a role in acute virulence. Swiss-Webster mice were infected intraperitoneally with 10 or 100 tachyzoites of WT or  $\Delta tln4$  parasites, and survival time was enumerated; 12 mice were infected for each strain and inoculum.

#### TLN4 does not contribute to invasion, replication, gliding motility, or virulence.

To assess whether TLN4 plays a role in the lytic cycle, plaque assays were performed. Compared to parental parasites,  $\Delta tln4$  parasites showed significantly smaller plaques (Fig. 4A and B), suggesting a defect in one or more steps in the parasite lytic cycle. This phenotype was fully restored in the complemented strain. We next tested each step in the lytic cycle to identify the basis of smaller plaques. Parasites deficient in TLN4 showed normal invasion (Fig. 4C) and replication at 17 h and 26 h postinfection (Fig. 4D), and all types of gliding motility were observed (Fig. 4E). Finally, no significant

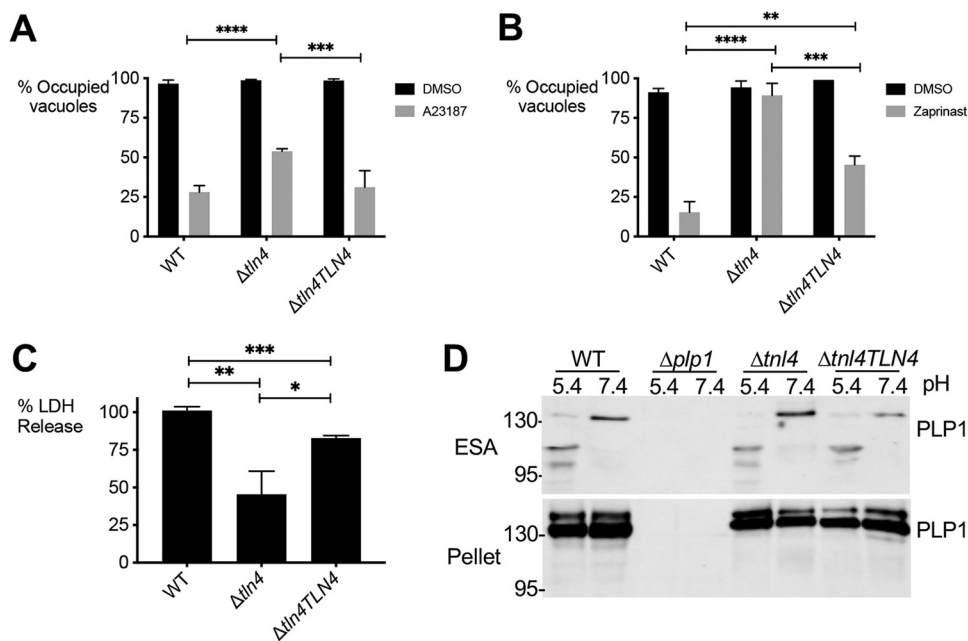


**FIG 5** *TLN4*-deficient parasites are defective in egress. (A and B) Parasite egress was quantified by immunofluorescence microscopy. Thirty-hour vacuoles were treated with DMSO or 2  $\mu$ M A23187 (A) or 200  $\mu$ M zaprinast (B) for 5 min prior to fixation and enumeration. \*,  $P \leq 0.05$ ; \*\*,  $P \leq 0.01$ ; \*\*\*,  $P \leq 0.001$ ; \*\*\*\*,  $P \leq 0.0001$ ; all by Student's *t* test. A minimum of 500 vacuoles were counted per strain. (C) Lactate dehydrogenase (LDH) release following induction with 100  $\mu$ M zaprinast was used as a measure of egress. Data are normalized to WT LDH release. All graphs shown are means  $\pm$  SEM from three biological replicates, each with triplicate samples. (D) Parasites lacking *TLN4* have normal PLP1 processing. Pellet and ESA were collected from parasites at pH 5.4 and 7.4, separated on SDS-PAGE, blotted onto membranes, and probed with rabbit anti-PLP1 antibodies. Processing of PLP1 in the ESA of all strains expressing PLP1 observed at pH 5.4. The pellet blot (bottom) acts as a loading control.

differences were observed in mouse survival of acute infection upon intraperitoneal infection with 10 or 100 tachyzoites (Fig. 4F).

***Δtln4* parasites are defective in efficient egress.** The last step of the lytic cycle is egress of the intracellular parasites from host cells, which can be induced by addition of the calcium ionophore A23187. Whereas most wild-type parasites egressed from host cells within 2 min of ionophore addition, at which time the cells were fixed, significantly fewer  $\Delta tln4$  parasites egressed in the allotted time (Fig. 5A). This phenotype is mostly reversed in  $\Delta tln4TLN4$  parasites. The deficiency in egress was more pronounced when zaprinast, a phosphodiesterase inhibitor, was used as an inducer (Fig. 5B), which may be due to its mode of action. Whereas A23187 elevates parasite cytosolic calcium by mobilizing it from parasite and host intracellular stores and the media, zaprinast treatment triggers the release of calcium from intracellular stores via activation of protein kinase G and inositol triphosphate signaling (4, 26). In this regard, zaprinast treatment likely better mimics the physiologic release of  $Ca^{2+}$  from intracellular stores during natural egress. An alternative and complementary measure of parasite egress is the release of host lactate dehydrogenase (LDH) into the surrounding medium due to loss of host cell integrity. After normalizing LDH release to WT parasites,  $\Delta tln4$  parasites showed ~45% release of LDH, while the complement strain nearly restored LDH release to wild-type levels (Fig. 5C). In examining the excreted-secreted antigen fraction of extracellular parasites, conducted in buffers with neutral or acidic pH (to mimic PV acidification [13–15]), there was no change in the processing of PLP1 in the  $\Delta tln4$  parasites compared to WT parasites (Fig. 5D). Together, these findings suggest a role for *TLN4* in *T. gondii* egress from host cells that is independent of PLP1 processing.

## DISCUSSION

*TLN4* was previously shown to be an extensively processed microneme protein (22), but its contribution to the lytic cycle was not determined due to the inability to

generate a knockout of this gene in the wild-type RH strain background. In this study, we were able to isolate a *TLN4* knockout strain by utilizing the more genetically tractable RH $\Delta ku80$  strain. Plaque assays showed that  $\Delta tln4$  parasites affected the lytic cycle, based on the smaller plaque sizes observed. Assessing the known steps of the lytic cycle showed that there were no defects in invasion, replication, or types of gliding motility performed by the parasites, and there was no effect on parasite virulence. The only deficiency observed was in induced egress, assessed by a static egress assay, and LDH release. Complementation of  $\Delta tln4$  with a *TLN4* construct under the control of the endogenous *TLN4* promoter fully restored the plaque defect and largely restored the egress deficiency.

*In vitro* investigation into *TLN4* suggests that the protein is an active protease based on cleavage of  $\beta$ -insulin as a model substrate, supporting a potential proteolytic function within the parasite. Homology modeling indicates that *TLN4* adopts the typical M16 structure and contains a catalytic chamber or “crypt,” which is one of the defining features of the M16 family of metalloproteinases. Studies with other M16 enzymes indicate that the crypt encapsulates and cleaves polypeptides, with the substrate being determined by the size and charge of the crypt as well as the flexibility of the substrate (s) (27, 28). Although it is possible that *TLN4* plays a direct role in egress by, e.g., facilitating the disruption of the PVM, an indirect contribution of *TLN4* to egress is also plausible. An indirect role could involve proteolytically activating another parasite protein that contributes to egress or degrading a protein that would otherwise compromise egress. Identifying substrates of *TLN4* in future studies might reveal the basis for its contribution to parasite exit from host cells.

PLP1 is the only microneme protein identified to date to have a direct role in egress. Interestingly, mice infected with  $\Delta tln4$  have no virulence defect, whereas  $\Delta plp1$  parasites are markedly virulence attenuated. This notable distinction could be because the egress defect of  $\Delta tln4$  parasites is less pronounced than that for  $\Delta plp1$ , or it could be due to additional roles for PLP1 during infection of mice. Future studies identifying other secretory proteins that contribute to egress to various degrees along with other work defining how PLP1 shapes the outcome of infection should help distinguish between these possibilities.

Among the Apicomplexa, the M16A subfamily is constrained to coccidian parasites, including close (e.g., *Hammondia hammondia* and *Neospora caninum*) and more distant (*Sarcocystis neurona* and *Eimeria* spp.) relatives of *T. gondii* (<https://orthomcl.org/orthomcl/app>). Whereas the genome of *T. gondii* encodes 11 M16 metalloproteinases, of which 4 belong to the M16A subfamily (29), the genome of the intestinal parasite *Cryptosporidium parvum* encodes an expanded family of 22 M16 metalloproteinases, 18 of which are M16A members. Among these, INS1 was recently shown to be necessary for formation of macrogamonts, the female sexual stage of *C. parvum* (30). The results of reciprocal BLAST searches indicate that *TLN4* is most closely related to *C. parvum* INS-15 (cgd3\_4260) and INS-16 (cgd3\_4270), which are closely related orthologs (83% identical) (30, 31). INS-15 localizes to the mid-apical region of *C. parvum* sporozoites and possibly merozoites (31). Antibodies to INS-15 impaired sporozoite cell invasion, suggesting a role in parasite entry into host cells. Future studies involving the targeted deletion of M16A family members in *C. parvum* and other coccidian parasites will be necessary to appreciate further their contributions to parasite infection biology.

## MATERIALS AND METHODS

**Structural modeling of *TLN4*.** The full amino acid sequence of ME49 strain *TLN4* was used to query Phyre2, which identified human insulin-degrading enzyme (PDB entry 2JBU) as the top-scoring template. This analysis resulted in a structural model of *TLN4* encompassing amino acids 202 to 1367. The structural model was visualized using PyMOL v2.3.2.

**Expression and purification of recombinant *TLN4*.** A region encoding domains A to IA-3 of the *TLN4* cDNA from RH strain (amino acids 209 to 1295) was amplified with *TLN4.625.NdeI.F* (5'-GGAA TTCATATGAGAGACACGAGCGCTACTCGG-3') and *TLN4.3885.NotR* (5'-AAGGAAAAAGCGGCCGCGCTAACCCACCGGAGGCGCTCGAGGAAAGC-3') primers and cloned into the bacterial expression vector pET21a,

introducing an in-frame C-terminal hexahistidine tag to the construct. The *Escherichia coli* expression construct containing the TLN4<sub>209-1295</sub> open reading frame (ORF) was verified by DNA sequencing.

The TLN4<sub>209-1295</sub> expression plasmid was transformed into *Escherichia coli* BL21 Gold cells selected on 2× yeast-tryptone (2YT) broth-agar plates containing 100 µg/ml ampicillin. Twenty milliliters of 2YT supplemented with ampicillin was grown to confluence overnight and then added to 1 liter of 2YT containing ampicillin and incubated with shaking at 37°C until an optical density at 600 nm (OD<sub>600</sub>) of ~0.85 was reached. Cultures were then induced with a final concentration of 1 mM isopropyl-β-D-thiogalactopyranoside (IPTG) overnight at 16°C.

Harvest and cell lysis of the overnight expression culture showed that TLN4<sub>209-1295</sub> expressed to high yields but was insoluble. Inclusion bodies were prepared by harvest of the insoluble fraction of the whole-cell lysate and resuspension with 30 ml of wash buffer I (25 mM Tris, pH 8.0, 300 mM NaCl, 1% Triton X-100). The suspension was homogenized until an even consistency was obtained. The inclusion bodies were then washed twice by centrifugation and homogenization in wash buffer I. Three subsequent washes with wash buffer II (25 mM Tris, pH 8.0, 300 mM NaCl) were performed to remove the excess Triton X-100. Purified inclusion bodies were stored at -80°C until required. Proteins were resolubilized in 25 mM Tris, pH 8.0, 250 mM NaCl, 6 M guanidine hydrochloride, 2 mM beta-mercaptoethanol by rotation at 4°C before centrifugation. Harvest supernatant was applied to nickel-nitrilotriacetic acid resin and purified via metal affinity chromatography. Purity of the denatured purified protein was assessed via SDS-PAGE and Western blotting.

Denatured TLN4<sub>209-1295</sub> was diluted to a final concentration of <1 mg/ml and applied dropwise to 100 ml of refold buffer (50 mM Tris, pH 8.2, 250 mM NaCl, 0.5 M arginine, 0.44 M sucrose, 4 mM reduced glutathione, 0.4 mM oxidized glutathione, 0.05 mM Tween 20) that was constantly stirring at 4°C. Refolding proceeded for 4 h at 4°C with gentle stirring. The refolded protein was then dialyzed overnight against 25 mM Tris, pH 8.0, 300 mM NaCl at 4°C. Postdialysis, the protein was concentrated to approximately 0.5 ml before application to a Superdex 200 10/300 column for further purification via size-exclusion chromatography.

**TLN4 proteolytic activity.** Hydrolysis of insulin B chain was measured via reverse-phase high-performance liquid chromatography (HPLC) following incubation of TLN4 (160 µg/ml) with insulin B chain (42 µM; Sigma-Aldrich) in 10 mM Tris for 88 h. HPLC was carried out in a Vydac C<sub>4</sub> HPLC column using a linear gradient from 0.1% trifluoroacetic acid (TFA) in 95% water, 5% acetonitrile to 0.1% TFA in 50% acetonitrile-water at a flow rate of 1 ml/min. Hydrolysis products were detected at 214 nm and collected for analysis. The obtained peptide products were analyzed on an Applied Biosystems 4800 matrix-assisted laser desorption ionization tandem time-of-flight proteomics analyzer at the University of Kentucky Proteomics Core.

**Parasite culture, transfection, and selection.** *T. gondii* tachyzoites were maintained by growth on monolayers of human foreskin fibroblasts (HFF) in Dulbecco's modified Eagle's medium (DMEM) containing 10% cosmic calf serum (GIBCO), 2 mM glutamine, 10 mM HEPES, 50 µg/ml penicillin-streptomycin (D10 Complete). To generate the TLN4 KO, a knockout construct (previously described in reference 22) containing 1.5 kb of TLN4 5' and 3' flanking regions was used, and the HXGPRT selectable marker was replaced with the DHFR-TS selectable marker cassette. This construct was transfected into RHΔku80Δhxg parasites with a Bio-Rad Gene Pulsar II with 1.5-kV voltage, 25-µF capacitance, and no resistance setting. Pyrimethamine selection was applied the day after transfection, and clones were isolated by limited dilution in 96-well plates. Knockout clones were tested for proper 5' integration, 5'-AGTTGCAGCCAGAGGAGCAAGTCC-3' (a) and 5'-CAGTCAGATAACAGGTGTAGCG-3' (b), and for proper 3' integration, 5'-GCGGTGACGCAGATGCGGTGTATCC-3' (c) and 5'-GAAAAGTGTCTGCTGTAGCAGC-3' (d). Knockout clones that were complemented with the TLN4.HA construct were identified with primers TLN4.322.F (e), 5'-GGCTTTCTGCTTCGTAAC-3', and TLN4.1910.R (f), 5'-AAGAGCAGTGGGCTGAAAA-3'.

The TLN4-IA<sup>1</sup>-HA<sup>2</sup> complementation plasmid was previously described in reference 22. This plasmid (50 µg) was cotransfected with 5 µg of the pDHFR-TS plasmid containing the selectable marker dihydrofolate reductase-thymidylate synthase by electroporation and drug selection with pyrimethamine. Positive clones were identified by PCR and Western blot analysis.

**Invasion assays.** Invasion assays were performed as previously described (32). Briefly, 1 × 10<sup>7</sup> parasites were used to infect subconfluent HFF monolayers in 8-well chamber slides for 20 min before fixation with paraformaldehyde. Slides were differentially stained with anti-SAG1 antibodies to differentiate attached versus invaded parasites.

**Egress assays.** Induced egress was performed as described previously (15). Briefly, parasites grown in HFFs in an 8-well chamber slide for 30 h were treated with 1% dimethyl sulfoxide, 2 µM A23187, or 200 µM zaprinast in assay buffer (Hanks' buffered salt solution containing 1 mM CaCl<sub>2</sub>, 1 mM MgCl<sub>2</sub>, and 10 mM HEPES) and incubated for 2 min in a 37°C water bath. Egress was stopped by addition of 2× fixative (8% formaldehyde in 1× PBS). Immunofluorescence was performed with rabbit anti-SAG1 to identify parasites and mouse anti-GRA7 (a generous gift from Peter Bradley) to identify the parasitophorous vacuole membrane. At least 10 fields of view (400× total magnification) per condition were enumerated as occupied or unoccupied.

LDH egress assays were performed as previously described (20). Briefly, parasites were grown in HFF monolayers in 96-well plates for 30 h. Wells were washed with Ringer's buffer and then treated with 100 µM zaprinast diluted in Ringer's buffer. Plates were incubated at 37°C for 20 min before removal and placement on ice. Fifty microliters of the supernatant were removed and centrifuged in a separate round-bottom plate. Thirty microliters of supernatant was subsequently removed and release of lactate dehydrogenase was determined using an LDH cytotoxicity colorimetric assay kit (BioVision).

**Plaque and replication.** Parasites were inoculated into wells of a 6-well plate and allowed to replicate undisturbed for 7 days. The wells were then stained with 0.2% crystal violet for 5 min and rinsed with double-distilled water (ddH<sub>2</sub>O). Images of the wells were scanned, and plaque number and size were analyzed with Image J.

For the replication assay, cells of an 8-well chamber slide were inoculated with  $1.25 \times 10^5$  tachyzoites and allowed to invade and grow for 17 h and 26 h prior to fixation and indirect immunofluorescence.

**Live gliding video microscopy.** Glass-well dishes (MatTek) were coated with 50% fetal bovine serum (FBS)–50% PBS overnight at 4°C or 1 h at 37°C and washed with PBS before use. Parasites were filter purified and resuspended in HHE (Hanks' salt solution, 10 mM HEPES, EDTA). Parasites were then added to coated dishes and allowed to settle for 5 min at room temperature. Dishes were then moved to a 37°C chamber with 5% CO<sub>2</sub> and warmed for 5 min prior to starting video recording. Each video consisted of 1 frame/s recorded for 90 s. Enumeration of the types of gliding motility were carried out by examining the videos in addition to maximum projection images generated by the Zeiss AxioVision software.

**Mouse infections.** All laboratory animal work in this study was carried out in accordance with policies and guidelines specified by the Office of Laboratory Animal Welfare, the U.S. Department of Agriculture, and the American Association for Accreditation of Laboratory Animal Care (AAALAC). The University of Michigan Committee on the Use and Care of Animals (IACUC) approved the animal protocol used for this study (Animal Welfare Assurance A3114-01, protocol no. PRO00008638). Freshly egressed parasites were filter purified in PBS, washed, counted, and injected intraperitoneally in 200  $\mu$ l of PBS into 6- to 8-week-old female Swiss Webster mice. The experiment was performed once with 4 groups of 12 mice each infected with 10 or 100 tachyzoites of WT or  $\Delta$ *tln4* parasites. Mice were given water and food *ad libitum*, monitored twice daily, and were humanely euthanized upon showing signs of morbidity.

**Western blotting.** Parasite lysates were generated by filter purifying parasites followed by centrifugation, 1  $\times$  wash with cold PBS, and resuspension in  $>90^\circ\text{C}$  1  $\times$  sample buffer. Lysates were boiled for 5 min prior to running on SDS-PAGE gels. Gels were semidry electroblotted (Bio-Rad) onto polyvinylidene fluoride membranes and sequentially probed with mouse anti-TLN4 (22) and horseradish peroxidase-conjugated goat anti-mouse (Jackson ImmunoResearch). Bands were revealed by enhanced chemiluminescence with SuperSignal West Pico Plus chemiluminescent substrate (Thermo Fisher Scientific) and documented with a Syngene Pxi imaging system.

**PLP1 processing.** Extracellular parasites ( $\Delta$ *ku80* $\Delta$ *hxg* [WT],  $\Delta$ *plp1*,  $\Delta$ *tln4*, and  $\Delta$ *tln4**TLN4*) were resuspended in PBS in either pH 5.4 or 7.4, and excreted-secreted antigen (ESA) was collected. Pellet lysates and ESA were separated on SDS-PAGE gels, and membranes were probed with antibodies against rabbit anti-PLP1.

## ACKNOWLEDGMENTS

This work was supported by National Institutes of Health grants R01AI46675 (V.B.C.) and 1R01GM130954 and 5P30GM110787 (L.B.H.). A.J.S. received fellowship support from the American Heart Association.

We thank Tracey L. Schultz for technical assistance.

## REFERENCES

1. Rock KL, Kono H. 2008. The inflammatory response to cell death. *Annu Rev Pathol* 3:99–126. <https://doi.org/10.1146/annurev.pathmechdis.3.121806.151456>.
2. Xia J, Cheng X-Y, Wang X-J, Peng H-J. 2017. Association between *Toxoplasma gondii* types and outcomes of human infection: a meta-analysis. *Acta Microbiol Immunol Hung* 64:229–244. <https://doi.org/10.1556/03064.2017.016>.
3. Bisio H, Soldati-Favre D. 2019. Signaling cascades governing entry into and exit from host cells by *Toxoplasma gondii*. *Annu Rev Microbiol* 73:579–599. <https://doi.org/10.1146/annurev-micro-020518-120235>.
4. Lourido S, Tang K, Sibley LD. 2012. Distinct signalling pathways control *Toxoplasma* egress and host-cell invasion. *EMBO J* 31:4524–4534. <https://doi.org/10.1038/emboj.2012.299>.
5. Wiersma HI, Galuska SE, Tomley FM, Sibley LD, Liberator PA, Donald RG. 2004. A role for coccidian cGMP-dependent protein kinase in motility and invasion. *Int J Parasitol* 34:369–380. <https://doi.org/10.1016/j.ijpara.2003.11.019>.
6. Garrison E, Treeck M, Ehret E, Butz H, Garbuz T, Oswald BP, Settles M, Boothroyd J, Arrizabalaga G. 2012. A forward genetic screen reveals that calcium-dependent protein kinase 3 regulates egress in *Toxoplasma*. *PLoS Pathog* 8:e1003049. <https://doi.org/10.1371/journal.ppat.1003049>.
7. Lourido S, Shuman J, Zhang C, Shokat KM, Hui R, Sibley LD. 2010. Calcium-dependent protein kinase 1 is an essential regulator of exocytosis in *Toxoplasma*. *Nature* 465:359–362. <https://doi.org/10.1038/nature09022>.
8. McCoy JM, Whitehead L, van Dooren GG, Tonkin CJ. 2012. TgCDPK3 regulates calcium-dependent egress of *Toxoplasma gondii* from host cells. *PLoS Pathog* 8:e1003066. <https://doi.org/10.1371/journal.ppat.1003066>.
9. Carruthers VB, Giddings OK, Sibley LD. 1999. Secretion of micronemal proteins is associated with *Toxoplasma* invasion of host cells. *Cell Microbiol* 1:225–235. <https://doi.org/10.1046/j.1462-5822.1999.00023.x>.
10. Carruthers VB, Moreno SN, Sibley LD. 1999. Ethanol and acetaldehyde elevate intracellular [Ca<sup>2+</sup>] and stimulate microneme discharge in *Toxoplasma gondii*. *Biochem J* 342:379–386. <https://doi.org/10.1042/0264-6021:3420379>.
11. Carruthers VB, Sibley LD. 1999. Mobilization of intracellular calcium stimulates microneme discharge in *Toxoplasma gondii*. *Mol Microbiol* 31:421–428. <https://doi.org/10.1046/j.1365-2958.1999.01174.x>.
12. Lovett JL, Marchesini N, Moreno SN, Sibley LD. 2002. *Toxoplasma gondii* microneme secretion involves intracellular Ca(2+) release from inositol 1,4,5-triphosphate (IP(3))/ryanodine-sensitive stores. *J Biol Chem* 277:25870–25876. <https://doi.org/10.1074/jbc.M202553200>.
13. Kafsack BF, Pena JD, Coppens I, Ravindran S, Boothroyd JC, Carruthers VB. 2009. Rapid membrane disruption by a perforin-like protein facilitates parasite exit from host cells. *Science* 323:530–533. <https://doi.org/10.1126/science.1165740>.
14. Roiko MS, Svezhova N, Carruthers VB. 2014. Acidification activates *Toxoplasma gondii* motility and egress by enhancing protein secretion and cytolytic activity. *PLoS Pathog* 10:e1004488. <https://doi.org/10.1371/journal.ppat.1004488>.
15. Roiko MS, Carruthers VB. 2013. Functional dissection of *Toxoplasma gondii* perforin-like protein 1 reveals a dual domain mode of membrane binding for cytolysis and parasite egress. *J Biol Chem* 288:8712–8725. <https://doi.org/10.1074/jbc.M113.450932>.

16. Bisio H, Lunghi M, Brochet M, Soldati-Favre D. 2019. Phosphatidic acid governs natural egress in *Toxoplasma gondii* via a guanylate cyclase receptor platform. *Nat Microbiol* 4:420–428. <https://doi.org/10.1038/s41564-018-0339-8>.
17. LaFavers KA, Marquez-Nogueras KM, Coppens I, Moreno SNJ, Arrizabalaga G. 2017. A novel dense granule protein, GRA41, regulates timing of egress and calcium sensitivity in *Toxoplasma gondii*. *Cell Microbiol* 19:10.1111/cmi.12749. <https://doi.org/10.1111/cmi.12749>.
18. Okada T, Marmansari D, Li Z, Adilbish A, Canko S, Ueno A, Shono H, Furuoka H, Igarashi M. 2013. A novel dense granule protein, GRA22, is involved in regulating parasite egress in *Toxoplasma gondii*. *Mol Biochem Parasitol* 189:5–13. <https://doi.org/10.1016/j.molbiopara.2013.04.005>.
19. Pzenny V, Ehrenman K, Romano JD, Kennard A, Schultz A, Roos DS, Grigg ME, Carruthers VB, Coppens I. 2016. A lipolytic lecithin:cholesterol acyltransferase secreted by *Toxoplasma* facilitates parasite replication and egress. *J Biol Chem* 291:3725–3746. <https://doi.org/10.1074/jbc.M115.671974>.
20. Schultz AJ, Carruthers VB. 2018. *Toxoplasma gondii* LCAT primarily contributes to tachyzoite egress. *mSphere* 3:e00073-18. <https://doi.org/10.1128/mSphereDirect.00073-18>.
21. Zhou XW, Kafsack BF, Cole RN, Beckett P, Shen RF, Carruthers VB. 2005. The opportunistic pathogen *Toxoplasma gondii* deploys a diverse legion of invasion and survival proteins. *J Biol Chem* 280:34233–34244. <https://doi.org/10.1074/jbc.M504160200>.
22. Laliberte J, Carruthers VB. 2011. *Toxoplasma gondii* toxolysin 4 is an extensively processed putative metalloproteinase secreted from micronemes. *Mol Biochem Parasitol* 177:49–56. <https://doi.org/10.1016/j.molbiopara.2011.01.009>.
23. Sidik SM, Huet D, Ganesan SM, Huynh MH, Wang T, Nasamu AS, Thiru P, Saeij JP, Carruthers VB, Niles JC, Lourido S. 2016. A genome-wide CRISPR screen in *Toxoplasma* identifies essential apicomplexan genes. *Cell* 166:1423–1435. <https://doi.org/10.1016/j.cell.2016.08.019>.
24. Hajagos BE, Turetzky JM, Peng ED, Cheng SJ, Ryan CM, Souda P, Whitelegge JP, Lebrun M, Dubremetz JF, Bradley PJ. 2012. Molecular dissection of novel trafficking and processing of the *Toxoplasma gondii* rhoptry metalloprotease toxolysin-1. *Traffic* 13:292–304. <https://doi.org/10.1111/j.1600-0854.2011.01308.x>.
25. Shen Y, Joachimiak A, Rosner MR, Tang W-J. 2006. Structures of human insulin-degrading enzyme reveal a new substrate recognition mechanism. *Nature* 443:870–874. <https://doi.org/10.1038/nature05143>.
26. McRobert L, Taylor CJ, Deng W, Fivelman QL, Cummings RM, Polley SD, Billker O, Baker DA. 2008. Gametogenesis in malaria parasites is mediated by the cGMP-dependent protein kinase. *PLoS Biol* 6:e139. <https://doi.org/10.1371/journal.pbio.0060139>.
27. Malito E, Hulse RE, Tang W-J. 2008. Amyloid  $\beta$ -degrading cryptidases: insulin degrading enzyme, presequence peptidase, and neprilysin. *Cell Mol Life Sci* 65:2574–2585. <https://doi.org/10.1007/s00018-008-8112-4>.
28. Stefanidis L, Fusco ND, Cooper SE, Smith-Carpenter JE, Alper BJ. 2018. Molecular determinants of substrate specificity in human insulin-degrading enzyme. *Biochemistry* 57:4903–4914. <https://doi.org/10.1021/acs.biochem.8b00474>.
29. Escotte-Binet S, Huguenin A, Aubert D, Martin A-P, Kaltenbach M, Florent I, Villena I. 2018. Metallopeptidases of *Toxoplasma gondii*: in silico identification and gene expression. *Parasite* 25:26. <https://doi.org/10.1051/parasite/2018025>.
30. Xu R, Feng Y, Xiao L, Sibley LD. 2021. Insulinase-like protease 1 contributes to macrogamont formation in *Cryptosporidium parvum*. *mBio* 12:e03405-20. <https://doi.org/10.1128/mBio.03405-20>.
31. Xu R, Guo Y, Li N, Zhang Q, Wu H, Ryan U, Feng Y, Xiao L. 2019. Characterization of INS-15, a metalloprotease potentially involved in the invasion of *Cryptosporidium parvum*. *Microorganisms* 7:452. <https://doi.org/10.3390/microorganisms7100452>.
32. Huynh MH, Rabenau KE, Harper JM, Beatty WL, Sibley LD, Carruthers VB. 2003. Rapid invasion of host cells by *Toxoplasma* requires secretion of the MIC2-M2AP adhesive protein complex. *EMBO J* 22:2082–2090. <https://doi.org/10.1093/emboj/cdg217>.